Macalester Journal of Physics and Astronomy

Volume 9
Issue 1 *Spring 2021*

Article 10

May 2021

Laser-Excitation Spectroscopy of Niobium Hydride and Tantalum Hydride

Siddhant Singh
Macalester College, ssingh1@macalester.edu

Laser-Excitation Spectroscopy of Niobium Hydride and Tantalum Hydride

Abstract

The experimental results presented in this paper shed light on some of the fundamental bonding characteristics of NbH and TaH. Six bands of niobium hydride and five weak bands of tantalum hydride were observed for the first time using laser excitation spectroscopy. The rotational assignments of observed bands were confirmed using dispersed fluorescence experiments for NbH and by checking the internal consistency of a global least squares fit for the weaker bands of TaH. For TaH, we were able to determine the term energies and molecular constants of each of its observed states to a high degree of accuracy by doing a combined global fit of the newly observed bands along with the previously known ones. For NbH, our preliminary experimental values compare well with computational predictions by Koseki et al. (2004). Upper states of both NbH and TaH show indications of perturbations with dark states. Further spectroscopy of NbH at higher wavelengths has to be carried out to characterize more electronic states.

Keywords

niobium hydride, tantalum hydride, laser-induced fluorescence spectroscopy

Cover Page Footnote

The research was funded by National Science Foundation and the Beltmann Fellowship. I would like to thank Professor Tom Varberg for his support during the research project as well as outside of it. I would also like to thank Zach Fried, who was my research partner for this project, as well as Ken Moffett, with whom we built some of the equipment that we installed in the lab. Finally, I would also like to thank professors and peers in the physics department for all that I have learned from them throughout my four years at Macalester.

Introduction

Group V metal monohydrides such as tantalum hydride (TaH), niobium hydride (NbH) and vanadium hydride (VH) have not had many experimental studies done on them, even though there have been a number of computational studies (Koseki et al., 2004; Das and Balasubramanian, 1990; Cheng and Balasubramanian, 1991). We believe the Varberg Lab is the first to have synthesized and recorded the spectra of both gaseous-phase TaH and NbH. The goal of our study was to find the energy levels of these molecules using laser-induced fluorescence spectroscopy such as laser excitation spectroscopy and dispersed fluorescence. TaH had been first synthesized in the Varberg lab in 2014 (Lee et al., 2014), and had more comprehensive work done on it in 2018-19 (Gleason et al., 2019). For the research covered in this paper, five weak bands of TaH were predicted using information from already known bands that had been seen using dispersed fluorescence and subsequently found experimentally using laser excitation spectroscopy. A global fit of the new states along with the existing states of TaH allowed us to verify the new assignments. Additionally, the lab also worked on characterizing the states of NbH. NbH had not been synthesized before and to the best of our knowledge we are the first to observe NbH. We have done a preliminary exploration of NbH so far, wherein we have discovered six bands in the range of 15400 - 17400 cm^{-1}.

The study primarily serves to increase fundamental knowledge about the bonding characteristics of TaH and NbH. Further, NbH also has resolvable hyperfine structure, which can provide valuable information about the valence electron wavefunctions for Group V metals (Varberg, personal communication). The Varberg lab also plans to record the spectra for VH, which could be of interest to astronomers since characteristic lines of VH might be seen in stellar spectra. The experiments also serve to verify the computational studies that had been conducted previously. In particular, we were interested in a study done by Mark Gordon and collaborators (Koseki et al., 2004) who had predicted the electronic spectra of gaseous group V hydrides using a variety of computational methods. The proposed potential energy curve for NbH from Koseki et al. is shown in Figure 1. We find that our experimental observations are in line with what was predicted, and we provide more accurate numbers for the term energies of low-lying states. Thus, our study allows us to make comparison between experimental values and computational predictions made using methods such as multi-configuration self-consistent field (MCSCF) calculations.

The excitation spectra are collected using laser excitation spectroscopy, which is described in the methods section. In terms of energy levels, rotational energy levels are a lot more closely spaced (on the order of 5-10 cm^{-1}) than vibrational levels (~1000 cm^{-1}) and electronic energy levels (~ 10000 cm^{-1}). The

resolution of the laser we use (Coherent 899 ring laser) is 0.001 cm^{-1}. Thus, our collected spectra clearly show the rotational levels.

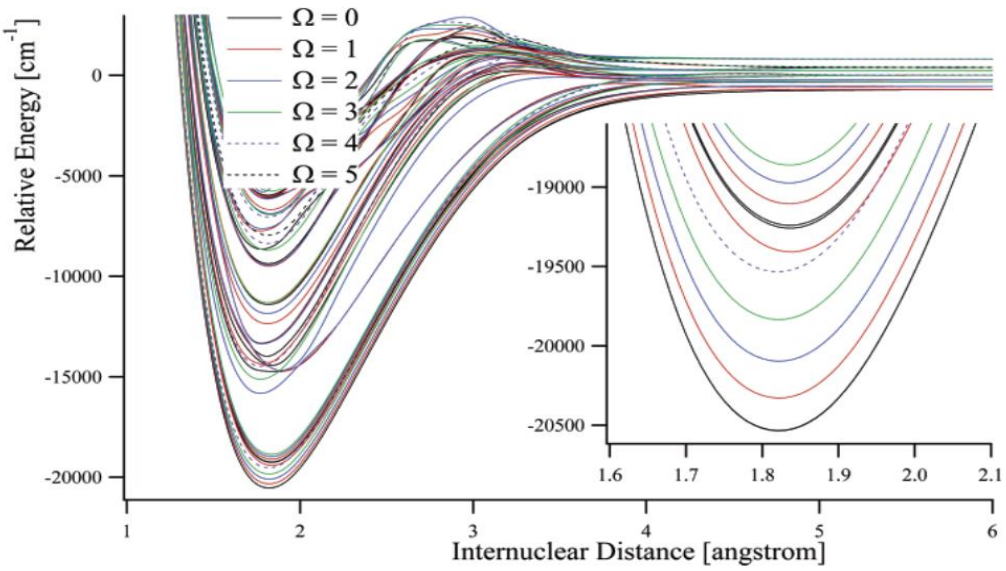

Figure 1: Predicted Potential Energy curve for NbH for low-lying spin-mixed states; predicted computationally. Figure from Koseki et al., 2004.

The assignment of the collected spectra is based on the rotational energy levels for a diatomic molecule obtained by solving Schrödinger's equation. Starting with a rigid rotor model and adjusting for centrifugal distortion, the rotational energy levels of a diatomic molecule are given by:

$$F(J) = BJ(J+1) - DJ^2(J+1)^2 \qquad (1)$$

Where J is the rotational quantum number, B is the rotational constant and D measures the magnitude of centrifugal distortion. The rotational constant is

inversely related to the square of the bond length of a particular state of the molecule:

$$B = \frac{\hbar}{4\pi c \mu r^2} \quad (2)$$

Where r is the bond length and μ is the reduced mass of the system.

The equation described above is not sufficient for certain states of NbH or TaH which have Ω-doubling, where Ω is the spin-orbit coupling. We will make some adjustments to the above equation for rotational energies for such states according to Hund's case (c) in our calculations later (Hougen and Wiersma, 2001).

As mentioned earlier, we use laser-induced fluorescence to collect the spectra, wherein we collect both excitation spectra through laser excitation spectroscopy and disperse spectra through dispersed fluorescence. Lasers are useful to get collimated and coherent light at high power. The principle behind the working of a laser is that if higher energy states have a larger population than lower energy states (a so-called *population inversion*), then stimulated emission of radiation can occur (Atkins and De Paula, 2014). We use a dye laser which can be used to scan over a range of wavelengths as the dye's interactions with the solvent broadens the range of light it can emit (Atkins and De Paula, 2014). Dyes we used included rhodamine-6G, which has a wavelength range of 570 nm – 650 nm, and DCM, which has a wavelength range of 610 nm – 710 nm (Dienes and Yankelevich, 1997). Dye lasers require another source to excite the dyes to a metastable state –

we achieve this excitation, or pumping, using a diode-pumped Verdi V10 laser (Verdi V10 - Coherent Inc. | *Laser*, n.d.).

Methodology

Production of Molecules

The molecules are produced using a hollow cathode discharge. The set-up is shown in Figure 2. The Group V metal electrode (the cathode) is placed in a chamber that is pumped with argon gas with trace amounts of hydrogen. A high voltage difference is applied between the cathode and a copper wire anode which results in the sputtering of atoms from the metal cathode due to collisions with Ar^+ ions. These metal atoms then combine with the hydrogen that is present in the chamber to form the metal hydride diatomic. While the discharge chamber mostly had TaH form with some TaO and TaN in the case of tantalum, significant amounts of both NbO and NbH formed when using a Nb electrode. Thus, while recording spectra for NbH, a balance between signal to noise had to be found where the noise was almost entirely due to the presence of NbO spectra. This was done by using an appropriate red pass filter and fine-tuning the current and pressure inside of the vacuum chamber. Moreover, we filtered the emitted radiation through a 1/8-m monochromator which acts as a narrow band-pass filter allowing us to reduce NbO signal (Varberg, personal communication).

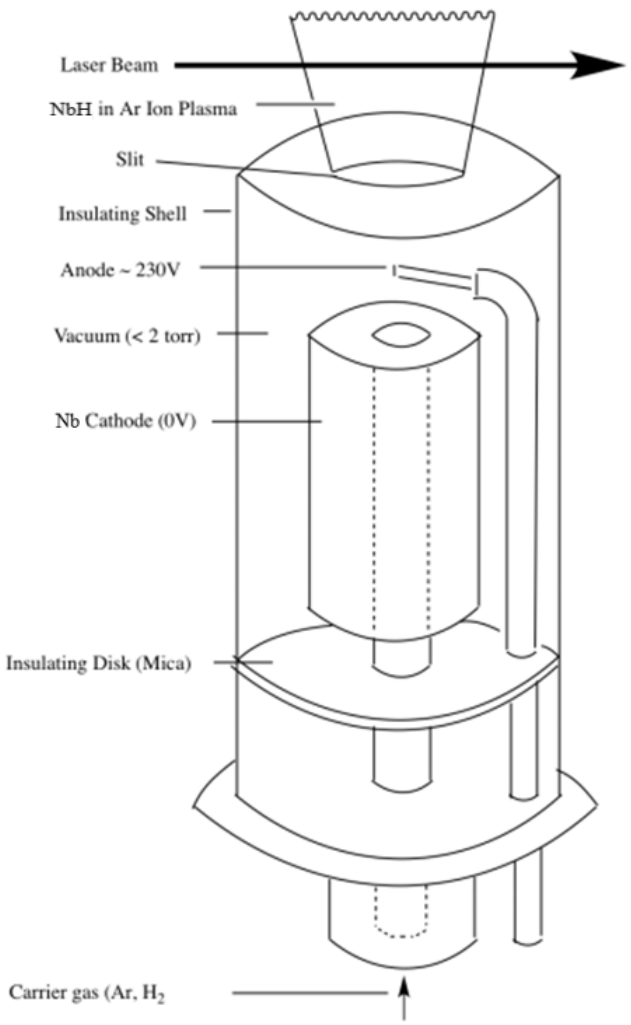

Figure 2: Hollow Cathode Discharge schematic. Figure adapted from Pearlman, 2016.

Spectroscopy Methods

A Coherent-899 CW ring laser is used to excite the produced molecules. It is a dye laser and we use organic dyes such as Kiton Red or Rhodamine 6-G depending on the range of wavelengths that are to be scanned. A 10W Verdi V10 green laser is used to pump the ring laser.

The spectra are recorded using laser excitation spectroscopy and the assignments are confirmed using dispersed fluorescence. In laser excitation spectroscopy, laser emission of a range of wavelengths (from the visible to a small part of the near infrared) is scanned and chopped before being double-passed through the discharge chamber where the molecule is being produced.

When the energy of the photons being sent through the laser matches the energy gap between any two states of the molecule, an electronic transition occurs. These electronic transitions are also accompanied by rotational and vibrational transitions. Since the resolution of our laser is about 0.001 cm^{-1}, rotational transitions are readily visible on the spectra we collect since the difference between rotational transition energies tends to be on the order of a few cm^{-1}. We can also observe vibrational transitions, though this was not something we were able to get to in the limited time of our research. While a number of molecules directly de-excite to their initial energy level, a considerable number also go to other low-lying states where transitions are allowed according to selection rules, as shown in Figure 3. This process is known as fluorescence. These molecules might then go back to the original state by non-radiative means (where the energy is often released as *phonons*, not photons). A Hamamatsu R928 photomultiplier tube (PMT) captures all the emitted fluorescent photons in our experimental set-up for laser excitation spectroscopy. The PMT converts the photons into a current and amplifies this observed signal. This method of laser excitation spectroscopy allows us to find the

energy differences of transitions from lower to higher levels, that is, the excitation energies (see Figure 3).

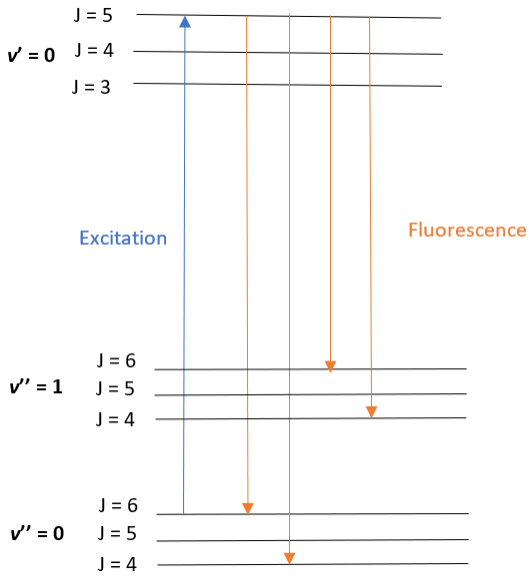

Figure 3: Energy level diagram demonstrating fluorescence. v'' is used to indicate the lower energy state in a vibrational transition, and v' the upper state.

The second method we use is dispersed fluorescence (DF). In this method, we focus the laser at a particular rotational line (picking one from amongst the excitation wavelengths we find in the excitation spectra) and then send the emitted light through a calibrated 0.75-m monochromator (Spex 750S) to find the intensities of individual fluorescent peaks. We pass this light through a Hamamatsu R943-02 PMT to amplify the signal. This method is based on the principle that once we excite a molecule to a higher state, it will fall back to a lower rotational state with $\Delta J = -1,\ 0, \text{or} +1$ where ΔJ is the change in rotational quantum number going

from a lower energy state to a higher energy state. This is referred to as the rotational selection rule and these transitions are respectively referred to as P, Q and R branches. Thus, if we were to excite a P(6) line, it would begin from $J_{i_1} = 6$ and end at $J_f = 5$. From $J_f = 5$, transitions can also occur to $J_{i_2} = 5$ or $J_{i_3} = 4$, corresponding to Q(5) and R(4) transitions respectively. The specific situation of fluorescence from a P(6) line is demonstrated in Figure 3. Note that the initial P(6) assignment had already been made using the laser excitation spectra. The spacing between the excited P(6) line and the corresponding Q and R lines at higher energies lets us confirm the initial assignment as we expect the distances between these lines to be specific multiples of *B*, the rotational constant.

Results and Discussion

TaH

Our work on TaH was continued from previous work of the lab, wherein the ground state and several low-lying electronic states had already been identified (Gleason et al., 2019). We were further able to identify five weak bands, which allowed us to do a global least-squares fit for all the known 17 bands and thus determine a consistent set of term energies and rotational constants for each of the observed bands (Fried et al., 2020). These new weak bands were found by predicting their location using the term energies and rotational constants that had been determined

in previous years' work on TaH through dispersed fluorescence (DF). The complete electronic states of TaH that we observed experimentally are shown in Figure 4.

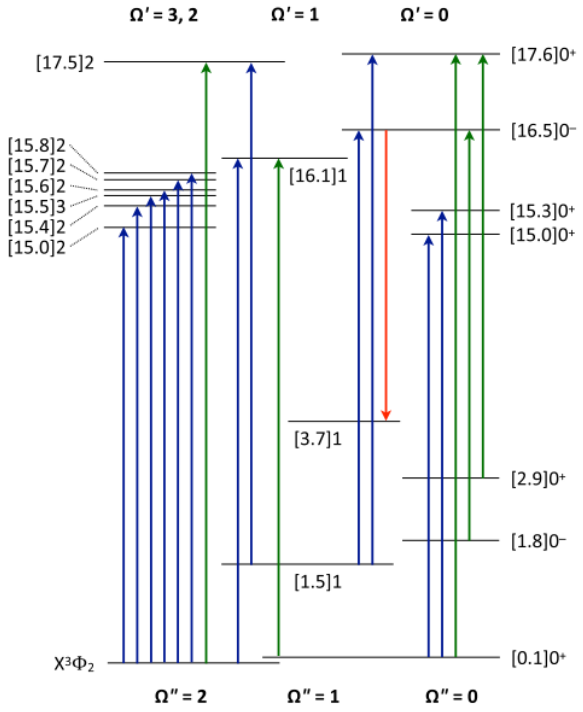

Figure 4: Energy level diagram for TaH reporting the states we have observed in lab. Ω'' represents lower energy states and Ω' the higher energy states in a transition. The numbers inside the square brackets represent the energy level of the state – for instance, the [15.4]2 state is observed somewhere in the 15400 cm^{-1} range and has Ω' = 2. The states with green arrows were observed during our work and the blue arrows had been seen previously. The red arrow state is only seen in dispersed fluorescence. Figure from Fried et. al (2020).

For TaH, the rotational energy within each electronic state was found using the following equation for Hund's case (c) (Hougen and Wiersma, 2001):

$$F(J)_f^e = T_v + BJ(J+1) - DJ^2(J+1)^2 \pm \frac{1}{2}q[J(J+1)]^{\Omega} \qquad (3)$$

Where the q term is for states with Ω-doubling.

Note that the identification of these new bands allowed us to reduce the error in our term energies from ± 3 cm^{-1} from previous work to ± 0.02 cm^{-1}, that is, an improvement by a magnitude of 100.

The calculated constants for the ground state of TaH as well as the low-lying states of the newly observed bands are presented in Table 1. We report the term energy (T_e), rotational constant (B), and centrifugal distortion constant (D) for each of the observed states, along with the q parameter for states with Ω-doubling.

State Label	T_e (cm^{-1})	B (cm^{-1})	D (cm^{-1})	q / cm^{-1}	q_D / cm^{-1}
$X^3\Phi_2$	[0]	5.448784(22)	$1.9115(27) \times 10^{-4}$	-	-
$[0.1]0^+$	80.4321(73)	5.38062(33)	$1.897(29) \times 10^{-4}$	-	-
[1.5]1	1458.620(10)	5.3218(12)	$1.61(35) \times 10^{-4}$	0.2123(11)	$1.89(44)*10^{-4}$
$[1.8]0^-$	1800.481(16)	5.4757(22)	$6.24(69) \times 10^{-4}$	-	-
$[2.9]0^+$	2895.821(16)	5.1981(26)	-	-	-

Table 1: Molecular constants for ground state of TaH as well as low-lying states involved in the newly observed bands.

NbH

We were able to observe six rotational bands for NbH in the 15400-17400 cm^{-1} range. A strong presence of NbO prevented us from differentiating between NbH and NbO lines at the initial stages of our experiment. We first observed peaks in the 16800 – 16900 cm^{-1} range while using a 780 nm bandpass filter – later dispersed fluorescence experiments revealed these to be $v = 2$ vibrational states.

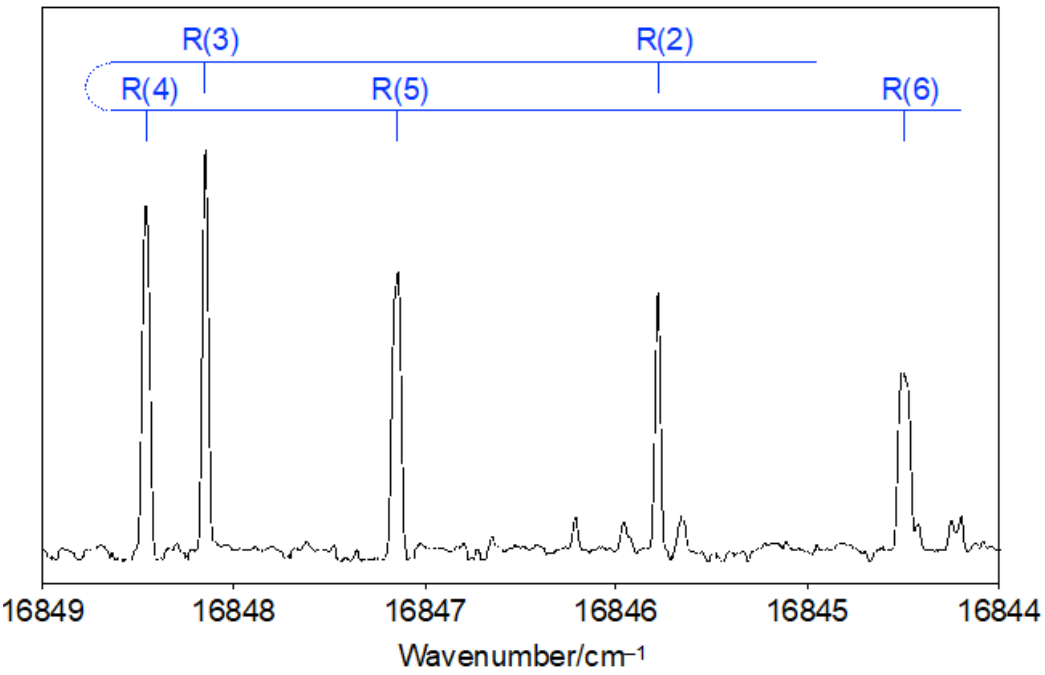

Figure 5: The R-branch of the [16.8] state. It is a Ω = 0-0 transition because there is no Q-branch in our spectra. Figure from Varberg, personal communication.

All of the six bands we observed were from the Ω'' = 0 ground state to an Ω' = 0 excited state. This was evident from the fact that we observed R(0) and P(1) lines and no Q-branch in our recorded spectra. Additionally, we were able to get a refined number for the first vibrational state for NbH. Our experiments found the vibrational spacing for the Ω'' = 0 ground state to be 1662 cm^{-1}, accurate to the accuracy of the monochromator in our DF experiments (3 cm^{-1}). The R-branch of the [16.8] state is shown in Figure 5. Once the bands had been recorded using laser excitation spectroscopy, the assignments were confirmed using dispersed fluorescence. The dispersed fluorescence of a P(6) line is shown in Figure 6.

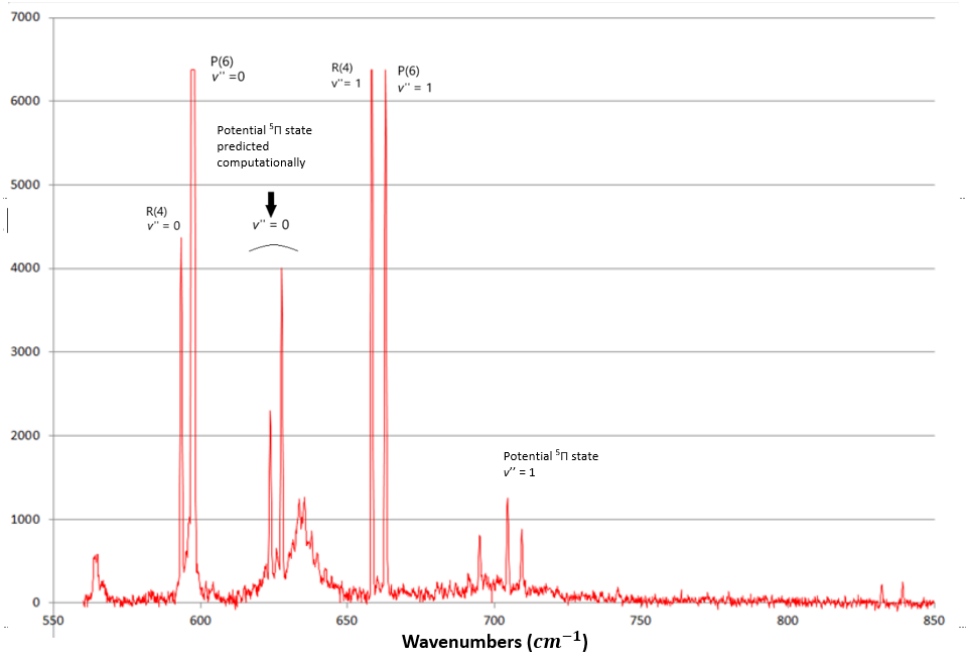

Figure 6: Dispersed Fluorescence (DF) spectra for a P(6) line. Fluorescence to v'' = 1 states can be seen. Other lines which match with computational predictions from Koseki et al. (2004) can also be seen but have not been confirmed.

We then fit our assigned peaks to the molecule's Hamiltonian using a least-squares fit, from which we obtained the term energy (T_e), rotational constant (B), and centrifugal distortion constant (D) for each of the states that we found. The bond length was also calculated from B. These data are presented in Table 2.

We observed that certain bands we recorded were perturbed, indicating the presence of dark states. These states do not show transitions from the ground states (and are thus "dark") but they interact with closely lying bright states, causing perturbations in the bright states we record.

State Label	T_e (cm^{-1})	B (cm^{-1})	D (cm^{-1})	Bond Length (Å)
$X^5\Delta_0$	0.0	4.9717	6.867×10^{-5}	1.844
[15.5]0	15461.743	5.0098	-5.928×10^{-6}	1.837
[15.8]0	15763.307	4.2001	4.312×10^{-4}	2.006
[16.0]0	15979.076	4.1657	-2.250×10^{-3}	2.015
[16.8]0	16839.561	5.1789	4.503×10^{-3}	1.807
[17.2]0	17249.536	4.7604	1.104×10^{-3}	1.885
[17.4]0	17399.673	3.9780	-2.996×10^{-3}	2.062

Table 2: Molecular constants for the observed bands of NbH. Since the bands are observed using laser excitation spectroscopy, the uncertainties for these constants are expected to be on the order of 0.001 cm^{-1}.

Future work

The next objective in the project is to find more bands for NbH at longer wavelengths. Moreover, the current set of spectra are Doppler-limited – in the future we would record sub-Doppler resolution spectra as well, allowing us to see the hyperfine structure of the molecule.

Furthermore, the Varberg lab has also recently synthesized Vanadium Hydride (VH) whose excitation bands need to be recorded and identified. The molecule could be of interest to astronomers who might find lines related to it in absorption spectra of stellar atmospheres. VH would also display hyperfine structure and would require sub-Doppler resolution spectra.

Acknowledgments

The research was funded by National Science Foundation and the Beltmann Fellowship. I would like to thank Professor Tom Varberg for his support during the research project as well as outside of it. I would also like to thank Zach Fried, who was my research partner for this project, as well as Ken Moffett, with whom we built some of the equipment that we installed in the lab. Finally, I would also like to thank professors and peers in the physics, chemistry, and mathematics (MSCS) department for all that I have learned from them throughout my four years at Macalester.

References

Atkins, P. W.; De Paula, J. Electronic Transitions. In *Physical Chemistry : Thermodynamics, Structure, and Change*, Tenth.; W.H. Freeman and Company: New York, 2014; pp 547-554.

Cheng, W.; Balasubramanian, K. Spectroscopic Constants and Potential Energy Curves for TaH. *Journal of Molecular Spectroscopy* **1991**, *149* (1), 99–108. https://doi.org/10.1016/0022-2852(91)90145-Z.

Dienes, A.; Yankelevich, D. R. 3 - Continuous Wave Dye Lasers. In *Experimental Methods in the Physical Sciences*; Dunning, F. B., Hulet, R. G., Eds.; Atomic, Molecular, and Optical Physics: Electromagnetic Radiation;

Academic Press, 1997; Vol. 29, pp 45–75. https://doi.org/10.1016/S0076-695X(08)60612-2.

Fried, Z. T. P.; Singh, S.; Varberg, T. D. Connecting All Electronic States of TaH: Observation of Five New Weak Bands. *Journal of Molecular Spectroscopy* **2020**, *372*, 111332. https://doi.org/10.1016/j.jms.2020.111332.

Gleason, S. P.; Kellett, D. H. P.; Reischmann, P. P.; Varberg, T. D. The Red Bands of TaH: Identification of the Ground and Low-Lying Electronic States. *Journal of Molecular Spectroscopy* **2019**, *362*, 56–60. https://doi.org/10.1016/j.jms.2019.05.012.

Hougen, J. and Wiersma, G. (2001), The Calculation of Rotational Energy Levels and Rotational Line Intensities in Diatomic Molecules, Monograph (NIST MN), National Institute of Standards and Technology, Gaithersburg, MD, [online], https://doi.org/10.6028/NBS.MONO.115 (Accessed March 28, 2021)

Koseki, S.; Ishihara, Y.; Fedorov, D. G.; Umeda, H.; Schmidt, M. W.; Gordon, M. S. Dissociation Potential Curves of Low-Lying States in Transition Metal Hydrides. 2. Hydrides of Groups 3 and 5. *J. Phys. Chem. A* **2004**, *108* (21), 4707–4719. https://doi.org/10.1021/jp049839h.

Lee, S. Y.; Christopher, C. R.; Manke, K. J.; Vervoort, T. R.; Varberg, T. D. The Electronic Spectrum of Tantalum Hydride and Deuteride. *Molecular*

Physics **2014**, *112* (18), 2424–2432. https://doi.org/10.1080/00268976.2014.906676.

Pearlman, Bradley, "High Resolution Electronic Spectroscopy of Gold Sulfide, AuS" (2016). *Chemistry Honors Projects*. 27. https://digitalcommons.macalester.edu/chem_honors/27

Varberg, T.D. Private Communication

Verdi V10 - Coherent Inc. | Laser https://www.gophotonics.com/products/lasers/coherent-inc-/29-263-verdi-v10 (accessed Mar 29, 2021).